


Quasinormal modes of spheroidal resonators in the null-field framework and application to hybrid anapoles

Benjamin Vennes¹ and Thomas C. Preston^{1,2,*}

¹*Department of Atmospheric and Oceanic Sciences, McGill University, 805 Sherbrooke Street West, Montreal, Quebec, H3A 0B9 Canada*

²*Department of Chemistry, McGill University, 805 Sherbrooke Street West, Montreal, Quebec, H3A 0B9 Canada*

 (Received 12 April 2022; accepted 29 June 2022; published 15 July 2022)

A model for calculating the quasinormal modes (QNMs) of homogeneous and core-shell spheroidal resonators is formulated in the null-field framework. Relying on a multipole expansion of the electromagnetic fields, the Mittag-Leffler theorem is employed to extract the QNMs from the poles of a response matrix. Physical quantities such as the extinction and scattering efficiency and the total internal energy of a mode are expressed directly in terms of the multipole expansion coefficients. We apply the model to study hybrid anapoles, which are radiationless states characterized by an enhancement of the total internal energy. Interference between excited QNMs and the background comprising of all other QNMs leads to a suppression of the extinction efficiency. Further, we show this suppression is due to Fano-like interference between resonant and background multipoles.

DOI: [10.1103/PhysRevA.106.013513](https://doi.org/10.1103/PhysRevA.106.013513)

I. INTRODUCTION

Quasinormal modes (QNMs) of dielectric resonators are the solutions to Maxwell's wave equation in the absence of a source. These modes couple with the external medium, so that they satisfy the outgoing wave condition. Consequently, the QNMs are the eigenstates of a nonconservative system, and so they possess complex eigenfrequencies, with the imaginary part related to the rate of dissipation of the mode in question [1]. These two considerations lead to the well-known issue that the electromagnetic fields are not square integrable in the usual sense because they become exponentially divergent at large distances away from the resonator [2,3]. To address this, normalization schemes have been proposed such as the use of perfectly matched layers to bound the domain of integration [4], a modified norm that bounds the problematic integral [5], or the use of the pole-response approach [6]. In this approach, the issue of normalizing diverging fields is avoided entirely by relying on the fact that QNMs are the poles of the scattering matrix [7]. Finally, an approach recently introduced circumvents the issue by regularizing the scattered field with a Green's approach [8].

In this report, we propose to use the null-field method [9]—sometimes referred to as the extended boundary condition method [10] or Waterman's T-matrix method [11]—to model spheroidal resonators in terms of its QNMs. This is combined with the so-called singularity expansion method (SEM) [12,13], whereby surface integral equations are used to avoid the issue of the diverging fields when reconstructing the scattered fields from the free space Green's function. This approach can be categorized as a pole-response method since the modes are determined from the singularities of a scattering operator. A key difference here with [13] is that the

SEM is applied to the response matrix instead of the surface currents. The response matrix relates the multipole expansion coefficients of an incident field to those of the internal field. In that sense, the proposed formalism builds upon the works of Colom and co-workers [14–16] that focused on the spectral expansion of Mie theory (spherical particles) and as such, this work constitutes an attempt to generalize the method to nonspherical homogeneous and core-shell geometries.

The model is applied to hybrid anapoles (HAs) in homogeneous and core-shell dielectric resonators. HAs are radiationless states characterized by an enhancement of the near and internal fields. For a homogeneous spherical particle, Mie theory allows for the straightforward determination of the anapole condition as cancellation in the far field will occur when the numerator of a scattering coefficient goes to zero. In the case of the electric dipole Mie scattering coefficient, this can be physically understood as resulting from the destructive interference in the far field from electric and toroidal dipole moments [17]. In the context of this Cartesian multipole decomposition, it was suggested that breaking the spherical symmetry of the particle or introducing a dielectric inhomogeneity allows for higher electric and toroidal moment to cancel out. It then follows that the HA condition is fulfilled when more than one moment is suppressed at a given wavelength [18–20].

An alternate perspective for investigating these states is the modal (or QNM) decomposition of the near and far fields. For a homogeneous spherical particle, it was recently shown that a Fano resonance formed by the interference between the resonant QNM and other QNMs along with a nonresonant contribution produces an anapole [21]. Using a QNM decomposition of the response matrix, it is first demonstrated with the model proposed here that HAs in spheroidal resonators are formed by two resonant QNMs of differing parity interfering with a background comprising all other QNMs. Then, with the multipole expansion of the QNM readily available, we

*thomas.preston@mcgill.ca

further demonstrate that this occurs when the suppression in the Fano-like interference between the resonant and background multipole moments coincide at a wavelength. Finally, since the far-field suppression at a given wavelength depends on the excitation of QNM resonances in the vicinity, the internal fields are found to be typically larger than the nonresonant background.

In Sec. II the surface integral approach used to model the QNMs is discussed. Then in Sec. III we employ the null-field method to transform the surface integral problem into a matrix problem. Finally, the response matrix obtained by the null-field method is expanded into its QNMs using the Mittag-Leffler theorem in Sec. IV. Validations of the model are presented in Sec. V, and lastly, the application to HAs is given in Sec. VI.

II. QNMs AND HUYGENS' PRINCIPLE

Huygens' principle for electromagnetic fields states that fields outside of a surface S enclosing an arbitrarily shaped particle can be represented by sets of radiating spherical wave sources distributed over the exterior of the surface. Inside of S , these sources interfere to produce the null field. Then, the Franz formula [22] which embodies the Huygens' principle allows for the scattered field \mathbf{E}_{sca} outside of an arbitrarily shaped particle to be expressed as

$$\begin{aligned} \nabla \times \int_S \mathbf{e}_{\text{sca}}(\mathbf{r}_S) g(k_0 R) dS - \frac{Z_0}{ik_0} \nabla \times \nabla \\ \times \int_S \mathbf{h}_{\text{sca}}(\mathbf{r}_S) g(k_0 R) dS = \begin{cases} \mathbf{E}_{\text{sca}}(\mathbf{r}), & \text{if } \mathbf{r} \text{ lies outside } S, \\ \mathbf{0}, & \text{if } \mathbf{r} \text{ lies inside } S, \end{cases} \end{aligned}$$

where $g(k_0 R)$ is the free space Green's function with $R = |\mathbf{r} - \mathbf{r}_S|$, \mathbf{r}_S is the position vector on the surface S , Z_0 is the impedance and k_0 is the wave number outside of the resonator. The tangential components of the electric and magnetic surface fields are $\mathbf{e}_{\text{sca}} = [\mathbf{n} \times \mathbf{E}_{\text{sca}}]_S$ and $\mathbf{h}_{\text{sca}} = [\mathbf{n} \times \mathbf{H}_{\text{sca}}]_S$. In the context of Huygens' principle, these tangential surface fields determine the strength of the spherical wave source on S which radiates according to the free space Green's function.

To construct a theory of QNMs in homogeneous and core-shell particles, the internal field in each layer are also expressed in terms of surface currents. Then the superposition principle is used to add these two equations. To be more succinct in our presentation, we define the following operators:

$$\begin{aligned} (\mathcal{M}_{ij}\mathbf{f})(\mathbf{r}) &= \nabla \times \int_{S_i} \mathbf{f}(\mathbf{r}_S) g(k_j R) dS, \\ (\mathcal{P}_{ij}\mathbf{f})(\mathbf{r}) &= \frac{Z_j}{ik_j} \nabla \times \nabla \times \int_{S_i} \mathbf{f}(\mathbf{r}_S) g(k_j R) dS, \end{aligned}$$

where \mathbf{f} represents the tangential electric field \mathbf{e} or the tangential magnetic field \mathbf{h} on the surface (the scattered or internal fields in either case). The QNMs of the homogeneous resonator are represented as

$$\begin{aligned} (\mathcal{M}_{10}\mathbf{e} - \mathcal{M}_{11}\mathbf{e})(\mathbf{r}) - (\mathcal{P}_{10}\mathbf{h} - \mathcal{P}_{11}\mathbf{h})(\mathbf{r}) \\ = \begin{cases} \mathbf{E}_{\text{sca}}(\mathbf{r}), & \text{if } \mathbf{r} \text{ lies outside } S, \\ \mathbf{E}_{\text{int}}(\mathbf{r}), & \text{if } \mathbf{r} \text{ lies inside } S. \end{cases} \end{aligned} \quad (1)$$

where 1 and 0 represents the interior and exterior, respectively. Imposing the continuity of the tangential component of the electromagnetic field on the surface of the resonator means that \mathbf{e} and \mathbf{h} can be written in terms of either the scattered or internal field. For the case of a core-shell particle, a similar set of expressions are given in Appendix A. Essentially, Eq. (1) can be used as a starting point to analyze QNMs. This is because, as per the definition of QNMs, (1) the Silver-Muller radiation condition is fulfilled by virtue of Green's function in free-space, and (2) the equation contains no source field.

III. THE NULL-FIELD METHOD

To proceed, the tangential electromagnetic fields need to be approximated in terms of a complete system of functions. We employ the null-field method in which the electromagnetic field are expanded in discrete source functions that satisfy the wave equation $\nabla \times \nabla \times \mathbf{F}(\mathbf{r}) = k^2 \mathbf{F}(\mathbf{r})$, where k is the wave number. One such set of discrete source functions, which will be used here, are the spherical vector wave functions (SVWFs) of polarization type TE, $\mathbf{M}_{lm}(k\mathbf{r})$, and TM, $\mathbf{N}_{lm}(k\mathbf{r}) = \nabla \times \mathbf{M}_{lm}(k\mathbf{r})/k$, where l is the mode number and m is the azimuthal mode number. Here it is convenient to incorporate the incident field in the analysis and express the tangential field in terms of the interior field:

$$\begin{aligned} (\mathcal{M}_{10}\mathbf{e}_{\text{int}} - \mathcal{M}_{11}\mathbf{e}_{\text{int}})(\mathbf{r}) - (\mathcal{P}_{10}\mathbf{h}_{\text{int}} - \mathcal{P}_{11}\mathbf{h}_{\text{int}})(\mathbf{r}) \\ = \begin{cases} \mathbf{E}_{\text{sca}}(\mathbf{r}), & \text{if } \mathbf{r} \text{ lies outside } S, \\ \mathbf{E}_{\text{int}}(\mathbf{r}) - \mathbf{E}_{\text{inc}}(\mathbf{r}), & \text{if } \mathbf{r} \text{ lies inside } S. \end{cases} \end{aligned} \quad (2)$$

Upon substitution of the field expansions into Eq. (2), the continuous surface integral equations are transformed into discretized matrix equations with $(\mathcal{M}_{10}\mathbf{e}_{\text{int}})(\mathbf{r}) - (\mathcal{P}_{10}\mathbf{h}_{\text{int}})(\mathbf{r}) \rightarrow -Q|\psi^{\text{int}}\rangle$, $\mathbf{E}_{\text{inc}} \rightarrow |\psi^{\text{inc}}\rangle$. So, in this quantum-like notation, we have

$$Q|\psi^{\text{int}}\rangle = |\psi^{\text{inc}}\rangle \quad \text{and} \quad |\psi^{\text{sca}}\rangle = -P|\psi^{\text{int}}\rangle, \quad (3)$$

where $|\psi^{\text{int}}\rangle$, $|\psi^{\text{inc}}\rangle$, and $|\psi^{\text{sca}}\rangle$ are the expansion coefficients of the internal, incident, and scattered fields in the basis of SVWFs. It follows that in the absence of the incident field, the expansion coefficients of the internal field of the n th QNM are the nontrivial solution to $Q(k_n)|\psi_n^{\text{int}}\rangle = 0$ where k_n is the n th resonant wave number (not to be confused with k_j , the wave number in the j th medium) and $|\psi_n^{\text{int}}\rangle$ is the right eigenvector. The right eigenvector $|\psi_n^{\text{int}}\rangle$ dictates the field distribution of the associated QNM inside the resonator. Since Q is non-Hermitian, there will also be the dual state $\langle \phi_n^{\text{int}} |$ which is the left eigenvector. The left eigenvector will determine how well the incident field couples into the QNM. In Appendix B we apply the null-field method to the core-shell resonator, and in Appendix C we discuss a solution to this nonlinear eigenproblem using an iterative procedure.

IV. THE SINGULARITY EXPANSION METHOD

Next the Mittag-Leffler theorem is used to expand the response matrix $R = Q^{-1}$ in terms of its poles, an approach commonly referred to as the singularity expansion method (SEM). Here the Mittag-Leffler theorem is applied to expand a matrix $R(k)$ analytic except at simple poles k_n with residue

matrices R_n as

$$R(k) = \sum_{s=0}^{p-1} \frac{R^{(s)}(k)}{s!} k^s + \sum_n \frac{R_n}{k - k_n} \left(\frac{k}{k_n} \right)^p, \quad (4)$$

where the parameter p is determined by the asymptotic behavior satisfying $\lim_{k \rightarrow \infty} |k^{-p} R(k)| = 0$. In Appendix D we show that $p = 1$ fulfills the requirement so that the expansion takes the form

$$R(k) = R(0) + \sum_n R_n \left(\frac{1}{k_n} + \frac{1}{k - k_n} \right). \quad (5)$$

We recall that the residue matrix, R_n , is given by the n th QNM projection matrix formed by the corresponding left and right eigenvectors

$$R_n = r_n |\psi_n^{\text{int}}\rangle \langle \phi_n^{\text{int}}|, \quad (6)$$

and where the pole residue r_n is given by

$$r_n = \frac{1}{\langle \phi_n^{\text{int}} | \frac{dQ}{dk} | \psi_n^{\text{int}} \rangle} \Big|_{k=k_n}. \quad (7)$$

We note that the denominator of the residue is nonzero for simple poles. However, in a non-Hermitian system, the eigenfrequencies and eigenvectors of two or more poles may coalesce and form a higher-order pole, called exceptional points of order N [23]. At these points, the first derivative vanishes, and so the Mittag-Leffler theorem would not be applicable in its given form. Barring this possibility, we perform some substitutions and find that the expansion coefficients of the internal field $|\psi^{\text{int}}(k)\rangle$ can be represented in terms of the QNMs as

$$|\psi^{\text{int}}(k)\rangle = \sum_n \left(\frac{r_n}{k - k_n} \right) |\psi_n^{\text{int}}\rangle \langle \phi_n^{\text{int}} | \psi^{\text{inc}}(k)\rangle, \quad (8)$$

in which we have established the completeness of the QNMs

$$R(0) + \sum_n \frac{R_n}{k_n} = 0, \quad (9)$$

which is shown in Appendix E. The scattered field expansion coefficients are obtained directly from the internal field expansions coefficients using

$$|\psi^{\text{sca}}(k)\rangle = -P(k) \sum_n \left(\frac{r_n}{k - k_n} \right) |\psi_n^{\text{int}}\rangle \langle \phi_n^{\text{int}} | \psi^{\text{inc}}(k)\rangle, \quad (10)$$

where $P(k)$ is the matrix that relates the internal state to the scattered state. It is noteworthy that, as in the case of the modal expansion of the surface currents [13], the electrostatic QNMs are not needed for calculating the internal energy or calculating far fields quantities such as the extinction and scattering efficiencies [24] and can be safely ignored here. Indeed, this differs from the more conventional approach of expanding the electromagnetic fields in QNMs directly. The choice of representing the expansion coefficients in QNMs is partly motivated by the fact that quantities of physical interest such as the total internal energy contained in the resonator, I_V , the extinction efficiency, Q_{ext} , and the scattering efficiency, Q_{sca} , can be computed directly from the field

coefficients:

$$I_V = \langle \psi^{\text{int}}(k) | I(k) | \psi^{\text{int}}(k)\rangle, \quad (11)$$

$$Q_{\text{ext}} = -\text{Re} \langle \psi^{\text{inc}}(k) | \psi^{\text{sca}}(k)\rangle / \pi x_{\text{eq}}^2, \quad (12)$$

$$Q_{\text{sca}} = \langle \psi^{\text{sca}}(k) | \psi^{\text{sca}}(k)\rangle / \pi x_{\text{eq}}^2, \quad (13)$$

where $I(k)$ is a matrix whose elements are volume integrals over the scalar product of two SVWFs [e.g., $I_{ll'mm'}^1(k) = 1/V \int_V \mathbf{M}_{lm}(\sqrt{\varepsilon} k \mathbf{r}) \cdot \mathbf{M}_{l'm'}^\dagger(\sqrt{\varepsilon} k \mathbf{r}) dV$ and V is the volume of the resonator] and x_{eq} denotes the volume equivalent size parameter. The calculations of these volume integrals are discussed in Appendix F. We note that in the case where the particle is spherical, the present framework becomes identical to the modal expansion of the Mie coefficients in a sphere [15]. However, a difference here is that the scattered state is obtained via the dispersive matrix $P(k)$ with no additional background to be included. On the other hand in [15], the scattered state is obtained directly from the QNMs but at the cost of a complex background which is needed to accurately reproduce the scattering profiles [21].

V. VALIDATION

We begin by validating the model for the case of an oblate dielectric spheroid with a permittivity $\varepsilon = 16$ and aspect ratio ranging from $h = 0.5$ to $h = 2$. In this case and in all subsequent ones, the incident beam $|\psi^{\text{inc}}\rangle$ is assumed to be an on-axis right-circular plane wave. Our focus is on axisymmetric particles, so the azimuthal mode number m remains a good number and the QNMs decouple according to their respective m . Consequently, the only QNMs that need to be considered in our calculations are the subset that couple with the incident field, here $m = 1$. Further, it is important to note that the mirror symmetry of the particles studied here reduces the QNMs of a subset m into two subsets which are independent of each other which we will call the parity.

In Figs. 1(a) and 1(b), the shift in the resonant size parameter of the dominant QNMs from that of the sphere are shown as a function of the aspect ratio of the spheroid. The QNMs are first determined for the analytical case of the sphere using Mie theory. In the nonspherical case, we preserve the convention of labeling the QNMs according to their polarization type (TE, TM) and mode assignment (l, m, ν) where l and m have the same definitions as earlier, and ν is the mode order (i.e., TE_{lm}^ν and TM_{lm}^ν). Then, once the QNMs of the sphere are known, the aspect ratio is varied in small increments and the homogeneous matrix equation is solved for the updated resonant wave number and eigenvectors. In Fig. 1(c) we compare the extinction efficiency of the QNM expansion versus the T-matrix method. We note that to achieve the good agreement between the two, we included some additional modes that lie outside the spectral range shown. The contribution of the individual QNMs to the overall extinction efficiency is also shown. It is noteworthy that the extinction profiles of the individual QNMs exhibit non-Lorentzian line shapes due to the dispersive effect of the matrix $P(k)$ acting on the QNM internal state $|\psi_n^{\text{int}}\rangle$.

In Fig. 2(a) we show the trajectory of the QNMs of a homogeneous polystyrene sphere in the complex plane as it deforms into a spheroid with an aspect ratio of $h = 1.2$. Polystyrene

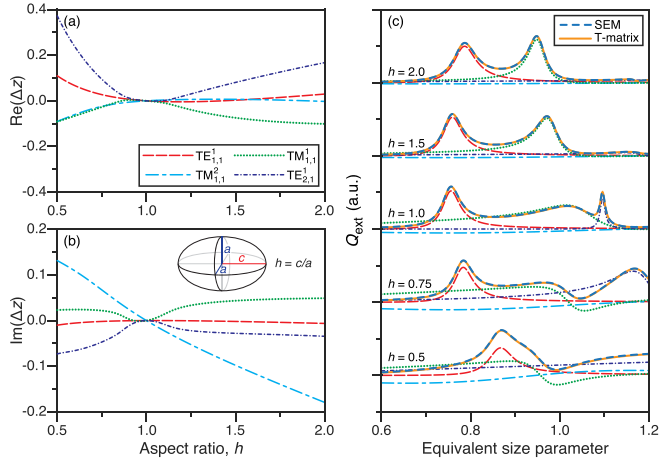


FIG. 1. The singularity expansion method (SEM) for oblate spheroids ($\varepsilon = 16$) with varying aspect ratio and a length scale similar to the wavelength. (a) The real part and (b) the imaginary part of the four QNMs that fall in the spectral range of interest as a function of the aspect ratio. (c) The extinction efficiency as a function of equivalent size parameter for a full T-matrix calculation, the SEM reconstruction, and the individual contribution from each QNM.

particles were chosen in this example as they are often used as a standard in light-scattering-based aerosol instruments [25] and are also ubiquitous in colloid and nanoscience. In this calculation, approximately 100 QNMs had to be included to properly replicate the extinction efficiency up to the equivalent size parameter of $x_{\text{eq}} \sim 10$ in Fig. 2(b). Concerning the trajectory of the QNMs in the complex plane, it is often argued that the dielectric sphere represent an ideal case for supporting QNMs, which would imply that any shape perturbation ought

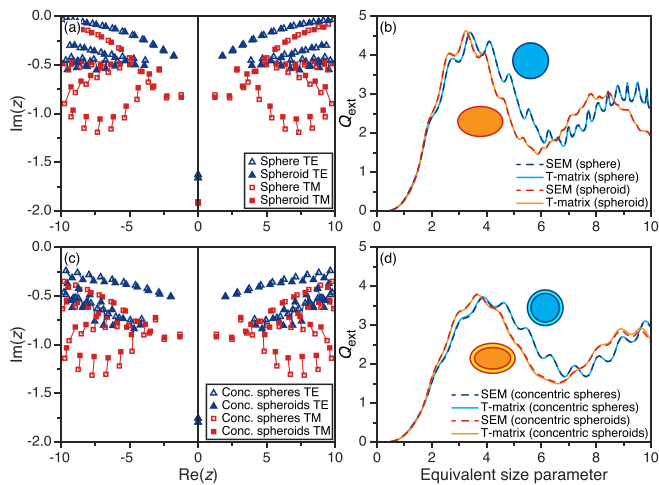


FIG. 2. The resonant size parameter of the QNMs of (a) a polystyrene sphere ($\varepsilon_{\text{ps}} = 2.517$) and (c) a water-coated ($\varepsilon_{\text{wat}} = 1.773$, core-shell ratio 0.75) polystyrene sphere as both systems are deformed into prolate concentric spheroids with $h = 1.2$. In (b) and (d), the extinction efficiency using the QNM expansion is compared to the T-matrix calculation for both the spherical and spheroidal particles.

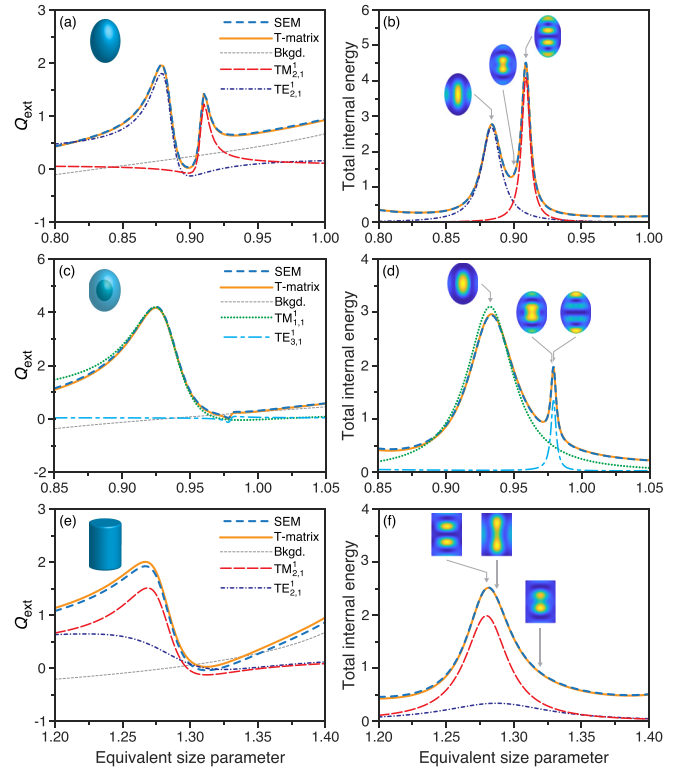


FIG. 3. The extinction efficiency (a, c, e) and total internal energy (b, d, f) of hybrid anapoles (HAs) in homogeneous and core-shell prolate spheroids. The extinction efficiency using the T-matrix method is compared against the SEM. Also shown are the extinction efficiency of the dominant QNMs and the so-called background, which is formed by the contribution of all other QNMs to the extinction efficiency. The total internal energy and the contributions from the dominant QNM are shown as well as the internal electric field distribution of the dominant QNMs and the anapole. The homogeneous spheroid in (a) and (b) has an aspect ratio $h = 1.575$ and permittivity $\varepsilon = 30$. The core-shell spheroid in (c) and (d) has an aspect ratio $h = 1.405$, core-shell ratio 0.5, and the permittivity of the core and shell are respectively $\varepsilon_{\text{core}} = 16$ and $\varepsilon_{\text{shell}} = 30$. In (e) and (f) the silicon cylinder is modeled using a superspheroid with $n_p = 64$, $h = 1.456$ and permittivity $\varepsilon = 14.977$.

to degrade the quality factor of the cavity relative to that of a sphere. As demonstrated in [26] and numerically investigated in [27], this is indeed the case provided the imaginary part of the complex size parameter is small. Here we see this systematically for the TE modes of the lowest mode order. For low-quality factor modes, we observe that deforming the sphere actually improves the quality factor, which concurs with the findings in [27]. Specifically, the TM modes of higher mode orders see their quality factor systematically improved as the sphere is deformed.

VI. APPLICATION TO HYBRID ANAPOLES

We now apply our model to reveal the modal content of HAs in homogeneous and core-shell spheroidal particles. Since optical anapoles are radiationless states, they can be located by looking for a vanishing extinction efficiency in calculated spectra. For instance, in Fig. 3 we investigated

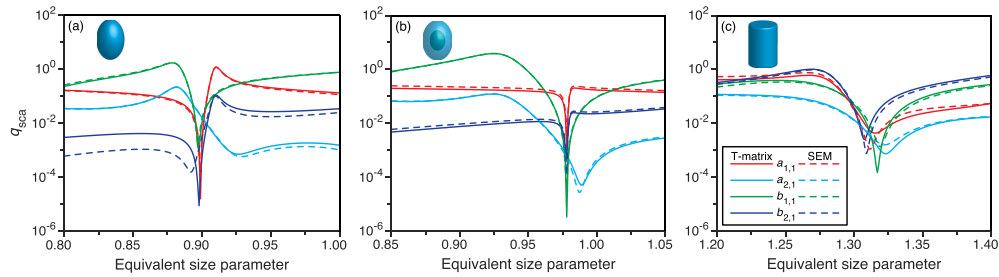


FIG. 4. The partial scattering efficiency, q_{sca} , of the first four multipole moments as a function of the equivalent size parameter in the vicinity of the hybrid anapoles in (a) the homogeneous spheroid, (b) core-shell spheroid, and (c) cylinder. The permittivities and parameters used to define the objects are identical to those listed in the caption of Fig. 3.

three cases where we observed a suppression of the extinction efficiency accompanied by an enhancement of the total internal energy at a given equivalent size parameter.

A noteworthy feature in Fig. 3 is that the extinction efficiency contribution from either the dominant modes or the background modes can drop below zero. The QNMs do not obey the usual Hermitian inner product but rather an unconjugated inner product. In the present case, however, the QNMs extracted from the response matrix, denoted as R_n , do not exhibit any orthogonality. This nonorthogonality of the QNMs can lead to negative extinction efficiency contributions, which arises due to interference effects between the nonorthogonal modes.

In Fig. 3(a) we observe that the anapole in the spheroid is formed by two QNMs, $TE_{2,1}^1$ and $TM_{2,1}^1$, which exhibit Fano-like profiles in their extinction efficiencies in the vicinity of $x_{eq} \sim 0.9$. To reproduce the original spectra, it is necessary to include the background formed by modes lying outside of the shown spectral range. In Fig. 3(b), due to the close proximity to the dominant QNMs, the total internal energy at the anapole position is enhanced in equal parts by the overlap of the two QNMs. Although the anapole lies at a local minimum between the two peaks, the total internal energy of the HA is still enhanced with respect to off-resonance conditions. The electric field distributions of the two QNMs as well as at the anapole are also shown in Fig. 3(b). Following the convention established by [20], the first resonance $TE_{2,1}^1$ is identified as a Mie-like resonance supported in an infinite cylinder while the second resonance $TM_{2,1}^1$ is akin to a Fabry-Perot mode formed by standing waves propagating from top to bottom in the spheroid.

The interpretations above can be carried over to anapoles in different structures such as the core-shell spheroid shown in Figs. 3(c) and 3(d). From the field distributions shown in 3(d), the $TM_{1,1}^1$ mode plays the role of the Mie-like mode while $TE_{3,1}^1$ that of the Fabry-Perot mode. In Fig. 3(c) both of these modes have negative extinction at the anapole $x_{eq} \sim 0.978$, which is compensated for by the background extinction formed by surrounding modes. In Fig. 3(d), while the anapole lies near the maximum of $TE_{3,1}^1$ mode, the effect of the broad $TM_{1,1}^1$ mode cannot be neglected in the total internal energy. In Figs. 3(e) and 3(f), we examine the case of a silicon cylinder as in [20] but with rounded edges. Again, the same pattern is observed in terms of the profile of the extinction efficiencies, wherein the $TE_{2,1}^1$ and $TM_{2,1}^1$ assume Fano-like profiles in the vicinity of the anapole $x_{eq} \sim 1.312$. From the electric field

energy distribution plots, we deduce the former mode is akin to the Fabry-Perot mode while the later is akin to the Mie-like mode. When examining the total energy at the anapole, both of these modes need to be considered in addition to the background.

A pattern that emerges from the above analysis is that at least two QNMs are involved in forming the anapole, one Mie-like and the other Fabry-Perot-like. In the present model, this can also be understood in terms of the so-called parity mentioned in Sec. V. To elaborate, the mirror-symmetry of the spheroid and the cylinder means the even TE modes do not couple with the odd TE modes and likewise for the TM modes. However, we note that even TE do couple with odd TM, and similarly for the odd TE and even TM. The point is that the two QNMs involved in forming the anapoles in Fig. 3 are independent from each other. In addition, this fact is important when considering the multipole content of each QNM. While the electric dipole and the magnetic quadrupole can mix, both are independent from the magnetic dipole and the electric quadrupole. This relation can be generalized to all electric and magnetic multipoles, in that even-numbered electric multipoles couple with odd-numbered magnetic multipoles, and likewise, odd-numbered electric multipoles couple with even-numbered multipoles. These two groups do not couple with each other. It is evident that, due to the mirror-symmetry of the resonators considered here, at least two QNMs of opposite parity are required in order for the first four multipole moments to vanish simultaneously.

The fact that the first four multipoles, namely, the electric and magnetic dipole moments and the electric and magnetic quadrupole moments, vanish in the vicinity of the HAs in Fig. 3 is confirmed in Fig. 4 for the three dielectric structures. In both the T-matrix calculation and the QNM reconstruction, the partial scattering efficiency, q_{sca} , contributed by each multipole is suppressed near the HA. In Fig. 5 we show that for the case of the homogeneous spheroid, the suppression of each partial scattering efficiency can be understood as a Fano-like resonance where the QNM nearest the HA provides the resonant multipole contribution while all other QNMs of the same parity provide the background multipole contribution. The minimum in the partial scattering efficiency of each multipole, denoted as gray vertical lines in the panels of Fig. 5 occurs when the resonant multipole partial scattering efficiency is approximately equal to the background multipole partial scattering efficiency. Then in Fig. 5 we demonstrate that this coincides with a phase difference $\Delta\phi \sim \pi$ where

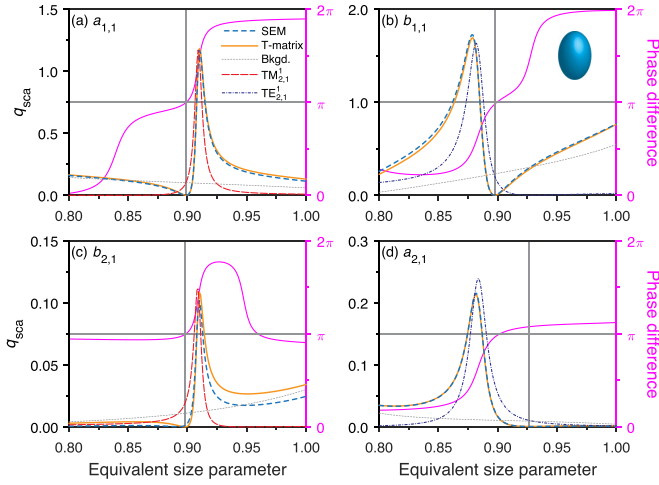


FIG. 5. The partial scattering efficiencies q_{sca} of each multipole and phase differences $\Delta\phi = \phi_{res} - \phi_{bkgd}$ between the resonant and background contributions of each multipole for the HA in the homogeneous spheroid. The vertical gray lines denote the minimum in the partial scattering efficiency. The horizontal gray lines denote a phase difference of π . The permittivities and parameters used to define the homogeneous spheroid are identical to those listed in the caption of Fig. 3.

$\Delta\phi = \phi_{res} - \phi_{bkgd}$ between the resonant multipole and background multipole. The antiphase condition is indicated in the figure with a gray horizontal line at $\Delta\phi = \pi$ in all the panels. This results in destructive interference and a nearly vanishing partial scattering efficiency. When the equivalent size parameter at which this occurs is roughly the same for each of the four multipoles, a hybrid anapole can be said to be formed. This investigation was also carried out for the first four multipoles

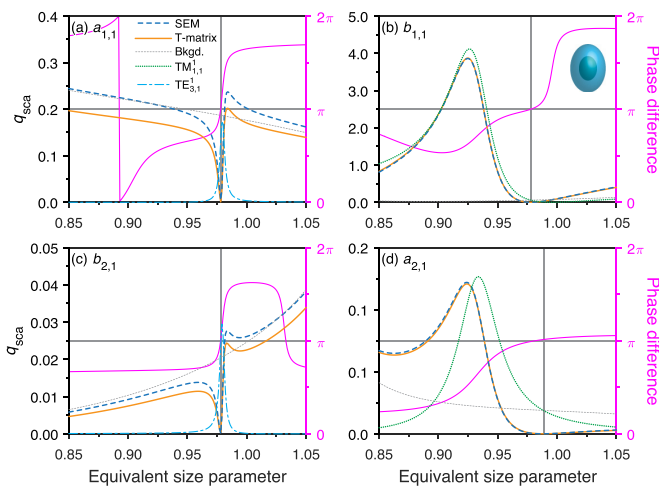


FIG. 6. The partial scattering efficiencies q_{sca} of each multipole and phase differences $\Delta\phi$ between the resonant and background contributions of each multipole for the HA in the core-shell spheroid. The vertical gray lines denote the minimum in the partial scattering efficiencies. The horizontal gray lines denote a phase difference of π . The permittivities and parameters used to define the core-shell spheroid are identical to those listed in the caption of Fig. 3.

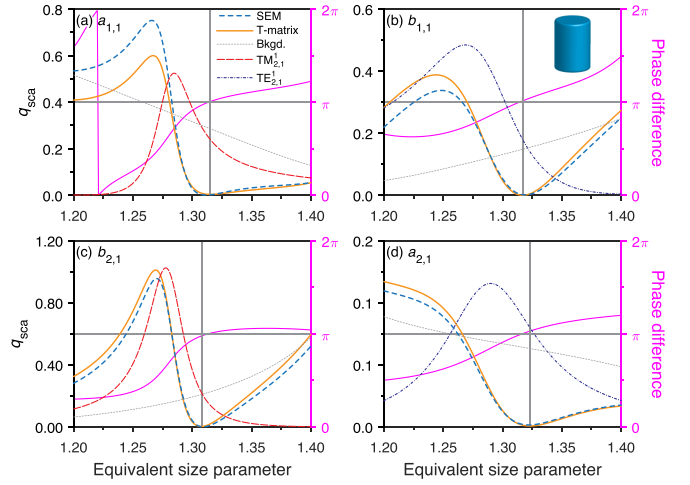


FIG. 7. The partial scattering efficiencies q_{sca} of each multipole and phase differences $\Delta\phi$ between the resonant and background contributions of each multipole for the HA in a cylinder. The vertical gray lines denote the minimum in the partial scattering efficiencies. The horizontal gray lines denote a phase difference of π . The permittivities and parameters used to define the cylinder are identical to those listed in the caption of Fig. 3.

in the other dielectric structures and the analogous results are presented in Figs. 6 and 7.

VII. CONCLUSIONS

A QNM theory based on the null-field method was presented for homogeneous and core-shell spheroidal particles. A distinctive feature of the current framework is that the modal expansion is carried out on the field coefficients instead of the electromagnetic vector fields and so it is a first attempt to extend the modal expansion of the Mie coefficients [15,28] to nonspherical geometries. The model was applied to the study of a few different systems, but our main focus was on the modal and multipole content of HAs. In general, the anapoles examined here arise when more than one multipole moment vanishes simultaneously near two independent QNMs of differing parity. We explained this by noting that each multipole moment vanishes due to Fano-like interference between the resonance of a nearby QNM and the background comprising other QNMs of the same parity. We conclude by emphasizing that the choice of discrete sources used in the null-field method is not limited to the spherical vector wave functions. Different discrete sources functions listed in [22] may be more appropriate for extreme geometries. However, if one restricts application to spheroids, a robust numerical implementation of the null-field method can be used [29] for extremely elongated or flattened spheroids.

ACKNOWLEDGMENT

T.C.P. acknowledges support from the Natural Sciences and Engineering Research Council of Canada (NSERC).

APPENDIX A: QUASINORMAL MODES (QNMs) AND HUYGENS' PRINCIPLE FOR CORE-SHELL RESONATORS

For a core-shell structure, the integral equations need to be modified in order to account for the inclusion of a second surface, namely, the core-shell interface. For clarity, we will identify the tangential electric and magnetic fields on the shell-medium interface as \mathbf{e}_s and \mathbf{h}_s and those on the core-shell interface as \mathbf{e}_c and \mathbf{h}_c . Then the first modification that is needed is to include an equation that gives the field inside the core

$$(\mathcal{P}_{22}\mathbf{h}_c)(\mathbf{r}) - (\mathcal{M}_{22}\mathbf{e}_c)(\mathbf{r}) = \begin{cases} \mathbf{0}, & \text{if } \mathbf{r} \text{ lies outside } S_2, \\ \mathbf{E}_{\text{core}}(\mathbf{r}), & \text{if } \mathbf{r} \text{ lies inside } S_2, \end{cases} \quad (\text{A1})$$

and in the case of the fields inside the shell, the addition of current fields associated with the core

$$\begin{aligned} & (\mathcal{M}_{21}\mathbf{e}_c - \mathcal{M}_{11}\mathbf{e}_s)(\mathbf{r}) - (\mathcal{P}_{21}\mathbf{h}_c - \mathcal{P}_{11}\mathbf{h}_s)(\mathbf{r}) \\ &= \begin{cases} \mathbf{0}, & \text{if } \mathbf{r} \text{ lies outside } S_1 \text{ or inside } S_2, \\ \mathbf{E}_{\text{shell}}(\mathbf{r}), & \text{if } \mathbf{r} \text{ lies between } S_1 \text{ and } S_2. \end{cases} \end{aligned} \quad (\text{A2})$$

So, by superposition, the QNMs of a core shell are

$$\begin{aligned} & (\mathcal{M}_{10}\mathbf{e}_s - \mathcal{M}_{11}\mathbf{e}_s + \mathcal{M}_{21}\mathbf{e}_c - \mathcal{M}_{22}\mathbf{e}_c)(\mathbf{r}) \\ & - (\mathcal{P}_{10}\mathbf{h}_s - \mathcal{P}_{11}\mathbf{h}_s + \mathcal{P}_{21}\mathbf{h}_c - \mathcal{P}_{22}\mathbf{h}_c)(\mathbf{r}) \\ &= \begin{cases} \mathbf{E}_{\text{sca}}(\mathbf{r}), & \text{if } \mathbf{r} \text{ lies outside } S_1, \\ \mathbf{E}_{\text{shell}}(\mathbf{r}), & \text{if } \mathbf{r} \text{ lies between } S_1 \text{ and } S_2, \\ \mathbf{E}_{\text{core}}(\mathbf{r}), & \text{if } \mathbf{r} \text{ lies inside } S_2. \end{cases} \end{aligned} \quad (\text{A3})$$

Therefore, the QNMs of a core-shell resonator can be represented using Huygen's principle by the addition of wave sources \mathbf{e}_c and \mathbf{h}_c associated to the core-shell interface. We note that boundary conditions for the tangential electric and magnetic fields on the surface and core-shell interface are needed in order to solve the integral equations.

APPENDIX B: THE NULL-FIELD METHOD

In the null-field method, a choice of discrete source functions are the localized spherical vector wave functions (SVWFs) of polarization type TE and TM. Respectively, these are represented in spherical coordinates (r, θ, ϕ) as [30]

$$\mathbf{M}_{lm}^{(j)}(k\mathbf{r}) = z_l^{(j)}(kr)[i\pi\tau_{lm}(\theta)\hat{\mathbf{e}}_\theta - \tau_{lm}(\theta)\hat{\mathbf{e}}_\phi]e^{im\phi}, \quad (\text{B1})$$

$$\begin{aligned} \mathbf{N}_{lm}^{(j)}(k\mathbf{r}) = & \left\{ l(l+1)\frac{z_l^{(j)}(kr)}{kr}P_{lm}(\theta)\hat{\mathbf{e}}_r \right. \\ & \left. + \frac{[krz_l^{(j)}(kr)]'}{kr}[\tau_{lm}(\theta)\hat{\mathbf{e}}_\theta + i\pi\tau_{lm}(\theta)\hat{\mathbf{e}}_\phi] \right\} e^{im\phi}, \end{aligned} \quad (\text{B2})$$

where the angular functions are given by

$$\pi\tau_{lm}(\theta) = \frac{m}{\sin\theta}P_{lm}(\theta) \quad \text{and} \quad \tau_{lm}(\theta) = \frac{d}{d\theta}P_{lm}(\theta), \quad (\text{B3})$$

and $P_{lm}(\theta)$ is the normalized associated Legendre polynomial. The radial function $z_l^{(j)}(kr)$ with $j = 1$ denotes the regular spherical Bessel function $z_l^{(1)} = j_l$, and with $j = 3$ the outgoing spherical Bessel function $z_l^{(3)} = h_l^{(1)}$. With this choice, the

internal and scattered fields for the homogeneous resonator are expanded in the embedded and circumscribing sphere, respectively,

$$\mathbf{E}_{\text{int}}(\mathbf{r}) = \sum_{l=1}^{\infty} \sum_{m=-l}^l c_{lm}\mathbf{M}_{lm}^{(1)}(k_1\mathbf{r}) + d_{lm}\mathbf{N}_{lm}^{(1)}(k_1\mathbf{r}), \quad (\text{B4})$$

$$\mathbf{E}_{\text{sca}}(\mathbf{r}) = \sum_{l=1}^{\infty} \sum_{m=-l}^l a_{lm}\mathbf{M}_{lm}^{(3)}(k_0\mathbf{r}) + b_{lm}\mathbf{N}_{lm}^{(3)}(k_0\mathbf{r}), \quad (\text{B5})$$

where the internal field coefficient and scattered field coefficients are unknown quantities to be determined. Additionally, the representation of the Green's dyadic in SVWFs is needed [31]

$$\begin{aligned} \vec{G}(kR) = & ik \sum_{l=1}^{\infty} \sum_{m=-l}^l \mathbf{M}_{lm}^{(3)*}(k\mathbf{r}')\mathbf{M}_{lm}^{(1)}(k\mathbf{r}) \\ & + \mathbf{N}_{lm}^{(3)*}(k\mathbf{r}')\mathbf{N}_{lm}^{(1)}(k\mathbf{r}), \quad |\mathbf{r}| < |\mathbf{r}'|, \end{aligned} \quad (\text{B6})$$

$$\begin{aligned} \vec{G}(kR) = & ik \sum_{l=1}^{\infty} \sum_{m=-l}^l \mathbf{M}_{lm}^{(1)*}(k\mathbf{r}')\mathbf{M}_{lm}^{(3)}(k\mathbf{r}) \\ & + \mathbf{N}_{lm}^{(1)*}(k\mathbf{r}')\mathbf{N}_{lm}^{(3)}(k\mathbf{r}), \quad |\mathbf{r}| > |\mathbf{r}'|, \end{aligned} \quad (\text{B7})$$

where \mathbf{r} and \mathbf{r}' are two arbitrary vectors in a free medium. We note complex conjugation applies only to the angular part of the SVWF and not the radial part. At this point, it is useful to also introduce the source field, which is assumed to be located exterior to the resonator and can be expanded in regular SVWFs as

$$\mathbf{E}_{\text{inc}}(\mathbf{r}) = \sum_{l=1}^{\infty} \sum_{m=-l}^l g_{lm}^{\text{TE}}\mathbf{M}_{lm}^{(1)}(k_0\mathbf{r}) + g_{lm}^{\text{TM}}\mathbf{N}_{lm}^{(1)}(k_0\mathbf{r}), \quad (\text{B8})$$

where g_{lm}^{TE} and g_{lm}^{TM} are the beam-shape coefficients for TE and TM polarizations, respectively. Then, in order to account for the incident field, the following Franz formula is used:

$$\begin{aligned} & (\mathcal{M}_{10}\mathbf{e}_{\text{inc}})(\mathbf{r}) - (\mathcal{P}_{10}\mathbf{h}_{\text{inc}})(\mathbf{r}) \\ &= \begin{cases} \mathbf{0}, & \text{if } \mathbf{r} \text{ lies outside } S_2, \\ -\mathbf{E}_{\text{inc}}(\mathbf{r}), & \text{if } \mathbf{r} \text{ lies inside } S_2. \end{cases} \end{aligned} \quad (\text{B9})$$

The standard procedure is to solve the following equation for the tangential surface fields:

$$\begin{aligned} & (\mathcal{M}_{10}\mathbf{e}_{\text{int}})(\mathbf{r}) - (\mathcal{P}_{10}\mathbf{h}_{\text{int}})(\mathbf{r}) \\ &= \begin{cases} \mathbf{E}_{\text{sca}}(\mathbf{r}), & \text{if } \mathbf{r} \text{ lies outside } S_1, \\ -\mathbf{E}_{\text{inc}}(\mathbf{r}), & \text{if } \mathbf{r} \text{ lies inside } S_1, \end{cases} \end{aligned} \quad (\text{B10})$$

where we emphasize that we are solving for the internal fields first by using $\mathbf{e} = \mathbf{e}_{\text{int}}$. With the SVWF expansions, the operator is replaced by a system of equations with $(\mathcal{M}_{10}\mathbf{e}_{\text{int}})(\mathbf{r}) - (\mathcal{P}_{10}\mathbf{h}_{\text{int}})(\mathbf{r}) \rightarrow -[Q_1^{31}]|\psi^{\text{int}}\rangle$, $\mathbf{E}_{\text{inc}} \rightarrow |\psi^{\text{inc}}\rangle$ and so, in this quantum-like notation, we have

$$[Q_1^{31}]|\psi^{\text{int}}\rangle = |\psi^{\text{inc}}\rangle \quad \text{and} \quad |\psi^{\text{sca}}\rangle = -[Q_1^{11}]|\psi^{\text{int}}\rangle, \quad (\text{B11})$$

where, for convenience, we assemble the expansion coefficients of the internal, incident and scattered fields in the bra-ket vectors $|\psi^{\text{int}}\rangle$, $|\psi^{\text{inc}}\rangle$, and $|\psi^{\text{sca}}\rangle$, respectively, and

introduced the matrix $[Q_i^{jk}]$ for the i th layer as

$$[Q_i^{jk}] = \begin{bmatrix} [K_i^{jk}] + \eta_i [J_i^{jk}] & [L_i^{jk}] + \eta_i [I_i^{jk}] \\ [I_i^{jk}] + \eta_i [L_i^{jk}] & [J_i^{jk}] + \eta_i [K_i^{jk}] \end{bmatrix}, \quad (\text{B12})$$

where $\eta_i = Z_{i-1}/Z_i$, Z_i is the impedance, and where the elements of the block matrices in Eq. (B12) are given by the following surface integrals:

$$[I_i^{jk}]_{ll'mm'} = ik_{i-1}^2 \int_{S_i} \mathbf{n}_i \cdot [\mathbf{M}_{lm}^{(j)*}(k_{i-1}\mathbf{r}_S) \times \mathbf{M}_{l'm'}^{(k)}(k_i\mathbf{r}_S)] dS,$$

$$[J_i^{jk}]_{ll'mm'} = ik_{i-1}^2 \int_{S_i} \mathbf{n}_i \cdot [\mathbf{M}_{lm}^{(j)*}(k_{i-1}\mathbf{r}_S) \times \mathbf{N}_{l'm'}^{(k)}(k_i\mathbf{r}_S)] dS,$$

$$[K_i^{jk}]_{ll'mm'} = ik_{i-1}^2 \int_{S_i} \mathbf{n}_i \cdot [\mathbf{N}_{lm}^{(j)*}(k_{i-1}\mathbf{r}_S) \times \mathbf{M}_{l'm'}^{(k)}(k_i\mathbf{r}_S)] dS,$$

$$[L_i^{jk}]_{ll'mm'} = ik_{i-1}^2 \int_{S_i} \mathbf{n}_i \cdot [\mathbf{N}_{lm}^{(j)*}(k_{i-1}\mathbf{r}_S) \times \mathbf{N}_{l'm'}^{(k)}(k_i\mathbf{r}_S)] dS.$$

Note that, when i appears in an expression, it is the imaginary number when it is neither a superscript nor a subscript. Therefore, in the absence of a source $|\psi^{\text{inc}}\rangle = 0$, the QNMs are the nontrivial solution to the homogeneous matrix equations with $Q = [Q_1^{31}]$ and $P = [Q_1^{11}]$

$$Q(k_n)|\psi_n^{\text{int}}\rangle = 0 \quad \text{and} \quad |\psi_n^{\text{sca}}\rangle = -P(k_n)|\psi_n^{\text{int}}\rangle. \quad (\text{B13})$$

The steps outlined for the homogeneous resonator are identical in the case of the core-shell resonator. However, the internal fields are separated into fields in the core and shell as follows:

$$\mathbf{E}_{\text{core}}(\mathbf{r}) = \sum_{l=1}^{\infty} \sum_{m=-l}^l c_{lm}^{(2)} \mathbf{M}_{lm}^{(1)}(k_2\mathbf{r}) + d_{lm}^{(2)} \mathbf{N}_{lm}^{(1)}(k_2\mathbf{r}), \quad (\text{B14})$$

$$\begin{aligned} \mathbf{E}_{\text{shell}}(\mathbf{r}) &= \sum_{l=1}^{\infty} \sum_{m=-l}^l c_{lm}^{(1)} \mathbf{M}_{lm}^{(1)}(k_1\mathbf{r}) + d_{lm}^{(1)} \mathbf{N}_{lm}^{(1)}(k_1\mathbf{r}) \\ &+ e_{lm}^{(1)} \mathbf{M}_{lm}^{(3)}(k_1\mathbf{r}) + f_{lm}^{(1)} \mathbf{N}_{lm}^{(3)}(k_1\mathbf{r}). \end{aligned} \quad (\text{B15})$$

For the core-shell resonator, the Q matrix is given by

$$Q_{\text{cs}} = [Q_1^{31}][Q_2^{31}] - [Q_1^{33}][Q_2^{11}], \quad (\text{B16})$$

and it relates the core field coefficients, denoted by $|\psi^{\text{int}}\rangle$ to the incident field coefficients, $|\psi^{\text{inc}}\rangle$. Here the P matrix is

$$P_{\text{cs}} = [Q_1^{11}][Q_2^{31}] - [Q_1^{13}][Q_2^{11}], \quad (\text{B17})$$

and it relates the core field coefficients to the scattered field coefficients $|\psi^{\text{sca}}\rangle$. In summary, we have

$$Q_{\text{cs}}|\psi^{\text{int}}\rangle = |\psi^{\text{inc}}\rangle, \quad \text{and} \quad |\psi^{\text{sca}}\rangle = -P_{\text{cs}}|\psi^{\text{int}}\rangle. \quad (\text{B18})$$

It is then clear that the QNMs are given by

$$Q_{\text{cs}}(k_n)|\psi_n^{\text{int}}\rangle = 0 \quad \text{and} \quad |\psi_n^{\text{sca}}\rangle = -P_{\text{cs}}(k_n)|\psi_n^{\text{int}}\rangle. \quad (\text{B19})$$

Finally, it is also desirable to know the field expansion inside the shell, as it can be used, for instance, to calculate the total internal energy. Both the regular $|\psi^{\text{shell,rg}}\rangle$ and outgoing component $|\psi^{\text{shell,out}}\rangle$ are related to the core coefficients through

$$|\psi^{\text{shell,rg}}\rangle = [Q_2^{31}]|\psi^{\text{int}}\rangle, \quad \text{and} \quad |\psi^{\text{shell,out}}\rangle = -[Q_2^{11}]|\psi^{\text{int}}\rangle. \quad (\text{B20})$$

APPENDIX C: NUMERICAL ROOT FINDING METHOD

The nontrivial solution to the homogeneous matrix equations yields both the eigenfrequency k_n and its eigenvector $|\psi_n^{\text{int}}\rangle$. In addition, the eigenvector $|\phi_n^{\text{int}}\rangle$ of the adjoint of the Q matrix is needed since the Q matrix is non-Hermitian, $\langle\phi_n^{\text{int}}|Q(k_n) = 0$. The algorithm used to determine the left eigenvector $|\phi_n^{\text{int}}\rangle$, right eigenvector $|\psi_n^{\text{int}}\rangle$, and the eigenfrequency k_n is the following iterative procedure [32]:

$$Q|\psi_n^{\text{int}}\rangle_{j+1} = \frac{dQ}{dk}|\psi_n^{\text{int}}\rangle_j, \quad (\text{C1})$$

$$Q^\dagger|\phi_n^{\text{int}}\rangle_{j+1} = \left(\frac{dQ}{dk}\right)^\dagger|\phi_n^{\text{int}}\rangle_j, \quad (\text{C2})$$

$$k_{n,j+1} = k_{n,j} - \frac{\langle\phi_n^{\text{int}}|Q|\psi_n^{\text{int}}\rangle_{j+1}}{\langle\phi_n^{\text{int}}|\frac{dQ}{dk}|\psi_n^{\text{int}}\rangle_{j+1}}. \quad (\text{C3})$$

At each iteration, the biorthogonal eigenvectors are renormalized to $\langle\phi_n^{\text{int}}|\psi_n^{\text{int}}\rangle = 1$ to avoid numerical overflow or underflow. The starting point of the iteration is the sphere, for which algorithms to determine the eigenfrequencies are well established. Here we use contour integration methods [33] along with the familiar Newton iteration [34,35]. To obtain the eigenfrequencies and eigenvectors of an arbitrarily shaped resonator, the sphere is deformed into the desired shape by small steps to ensure convergence of the iteration.

APPENDIX D: THE SINGULARITY EXPANSION METHOD

It has been shown that the zeros of the Q matrix correspond to the QNMs of the resonator, and its associated eigenfrequencies and eigenvectors may be determined by iterative procedures in Appendix C. Once these quantities are known, a modal decomposition of the internal and scattered field expansion coefficients in the presence of a source exterior to the resonator is accomplished by using the singularity expansion method.

Let $R(k) = Q^{-1}(k)$ be an analytic matrix in k with simple poles k_n (and otherwise invertible at all k) and a corresponding residue matrices R_n . Then the Mittag-Leffler theorem states that for an integer p and a uniform bound M such that $\max|k^{-p}R| < M$ on C_m as $m \rightarrow \infty$ (C_m is a circle on the complex plane centered on $k = 0$ with radius $R_m \rightarrow \infty$ as $m \rightarrow \infty$), $R(k)$ has the following representation:

$$R(k) = \sum_{s=0}^{p-1} \frac{R^{(s)}(k)}{s!} k^s + \sum_n \frac{R_n}{k - k_n} \left(\frac{k}{k_n}\right)^p. \quad (\text{D1})$$

In order to construct a pole expansion of the R matrix, the integer p at which Eq. (D1) is truncated needs to be determined. This is accomplished by examining the asymptotic limit $\lim_{k \rightarrow \infty} Q(k)$. In the framework of the null-field method, it turns out that $p = 1$ yields the correct asymptotic limit for both the core-shell and homogeneous Q matrix. In the case of a homogeneous resonator or particle, the functional dependence of a typical entry of the Q matrix with respect to k is a product of a spherical Bessel and a spherical Hankel function

$$Q_{l'l'} \sim nz^2 j_{l'}(nz) h_l(z), \quad (\text{D2})$$

where n is the refractive index of the homogeneous particle. For a fixed $l < L$ and $l' < L$ where $L \ll z$, we may exploit the asymptotic formula of the spherical Bessel and Hankel functions as $z \rightarrow \infty$ and $z \gg L$. This yields

$$nz j_{l'}(nz) \sim e^{inz} + e^{-inz} \quad \text{and} \quad zh_l(z) \sim e^{iz}, \quad (\text{D3})$$

so that the asymptotic form of the product is expressed with complex exponentials as

$$Q_{ll'} \sim ae^{i(n+1)z} + be^{-i(n-1)z}, \quad (\text{D4})$$

where a and b are constants that are of no importance. For a real-valued positive definite permittivity, it turns out that this asymptotic limit admits only oscillatory terms on the real axis $\text{Re}(z)$. In general, on the complex plane, the asymptotic limit will be dominated by the exponential growth. Then, the inverse $R = Q^{-1}$ will have exponential decay in the complex plane and will remain oscillatory on the real axis. Therefore, the Mittag-Leffler theorem with $p = 1$ will suffice to reproduce this behavior because $\max |k^{-1}R| < M$ on C_m as $R_m \rightarrow \infty$ and thus

$$R(k) = R(0) + \sum_n R_n \left[\frac{1}{k - k_n} + \frac{1}{k_n} \right]. \quad (\text{D5})$$

Now, we need to determine the residue matrix. With a bit of work, the residue matrix is expressed in terms of the projection matrix of Q . Assume a Laurent series of the $R = Q^{-1}$ matrix about $k = k_n$ as

$$Q^{-1} = \frac{R_n}{k - k_n} + A_0 + (k - k_n)A_1 + \dots, \quad (\text{D6})$$

where A_0, A_1, \dots represent matrices of no importance in the final expression and we assume a simple pole at $k = k_n$ for consistency. If we then differentiate with respect to k we get

$$\frac{d}{dk} Q^{-1} = -Q^{-1} \frac{dQ}{dk} Q^{-1} = \frac{-R_n}{(k - k_n)^2} + A_1 + \dots \quad (\text{D7})$$

This can be reorganized to yield

$$(k - k_n)Q^{-1} \frac{dQ}{dk} (k - k_n)Q^{-1} = R_n - A_1(k - k_n)^2 - \dots, \quad (\text{D8})$$

and we may proceed to evaluate the limit as $k \rightarrow k_n$. We will need the spectral representation of Q^{-1} which is

$$Q^{-1} = \sum_j \frac{1}{\lambda_j} |\psi_j\rangle \langle \phi_j|, \quad (\text{D9})$$

where λ_n is the n th eigenvalue of

$$Q|\psi_n\rangle = \lambda_n|\psi_n\rangle = 0 \quad \text{as } k \rightarrow k_n, \quad (\text{D10})$$

$$\langle \phi_n|Q = \lambda_n\langle \phi_n| = 0 \quad \text{as } k \rightarrow k_n. \quad (\text{D11})$$

The limit will yield the residue matrix in terms of the projection matrix

$$R_n = \lim_{k \rightarrow k_n} \sum_j \frac{k - k_n}{\lambda_j} |\psi_j\rangle \langle \phi_j| = \delta_{nj} r_n |\psi_n\rangle \langle \phi_n|, \quad (\text{D12})$$

where r_n denotes the pole residue at $k = k_n$ and δ_{nj} is the Kronecker delta function. However, it also follows from the

differentiation that the residue matrix can be expressed as

$$R_n = r_n^2 |\psi_n^{\text{int}}\rangle \langle \phi_n^{\text{int}}| \frac{dQ}{dk} |\psi_n^{\text{int}}\rangle \langle \phi_n^{\text{int}}|, \quad (\text{D13})$$

which means that the pole residue r_n is given by

$$r_n = \frac{1}{\langle \phi_n^{\text{int}}| \frac{dQ}{dk} |\psi_n^{\text{int}}\rangle}, \quad (\text{D14})$$

and so the residue matrix is

$$R_n = \frac{|\psi_n^{\text{int}}\rangle \langle \phi_n^{\text{int}}|}{\langle \phi_n^{\text{int}}| \frac{dQ}{dk} |\psi_n^{\text{int}}\rangle}. \quad (\text{D15})$$

Then we find that the pole expansion of the R matrix is

$$R(k) = R(0) + \sum_n r_n \left(\frac{1}{k - k_n} + \frac{1}{k_n} \right) |\psi_n^{\text{int}}\rangle \langle \phi_n^{\text{int}}|. \quad (\text{D16})$$

Therefore, the expansion of the internal field $|\psi^{\text{int}}(k)\rangle$ is given by operating the singularity expansion of $R(k)$ onto $|\psi^{\text{inc}}(k)\rangle$, which yields

$$\begin{aligned} |\psi^{\text{int}}(k)\rangle &= R(0)|\psi^{\text{inc}}(k)\rangle \\ &+ \sum_n r_n \left(\frac{1}{k - k_n} + \frac{1}{k_n} \right) |\psi_n^{\text{int}}\rangle \langle \phi_n^{\text{int}}| \psi^{\text{inc}}(k). \end{aligned} \quad (\text{D17})$$

Unless indicated, the vectors and matrices are evaluated at $k = k_n$. This concludes the problem of determining the fields in terms of the zeros of the Q matrix (or the poles of the R matrix). The scattered field is obtained by $|\psi^{\text{sca}}(k)\rangle = -P(k)|\psi^{\text{int}}(k)\rangle$.

In the case of the core-shell resonator, some simplifications will be useful. First, we begin with

$$Q_{\text{cs}} = Q_1^{33} Q_2^{11} - Q_1^{31} Q_2^{31} = i[Q_1^{32} Q_2^{11} - Q_1^{31} Q_2^{32}], \quad (\text{D18})$$

In the asymptotic limits with $l < L$ where $L \ll z$, we will have

$$z j_l(z) \sim \cos(z), \quad z y_l(z) \sim \sin(z), \quad \text{and} \quad z h_l(z) \sim e^{iz}. \quad (\text{D19})$$

Therefore,

$$\begin{aligned} Q_{\text{cs},ll'} &\sim e^{iz_1} \cos(n_2 z_2) \\ &\times [a \sin(n_1 z_1) \cos(n_1 z_2) - b \sin(n_1 z_2) \cos(n_1 z_1)], \end{aligned} \quad (\text{D20})$$

which will have exponential growth on the complex plane and remain oscillatory on the real-axis. Now, for the purpose of calculating the total internal energy contribution from the shell, we need to check whether $p = 1$ is sufficient. Recall from Eq. (B20) that the outgoing component of the shell field was given by the matrix $[Q_2^{11}]^{-1} Q_{\text{cs}}$ so that the asymptotic limit goes as

$$\begin{aligned} [Q_2^{11}]_{ll'}^{-1} Q_{\text{cs},ll'} &\sim ae^{iz_1} \sin(n_1 z_1) \\ &- be^{iz_1} \sin(n_1 z_2) \cos(n_1 z_1) / \cos(n_1 z_2). \end{aligned} \quad (\text{D21})$$

For $z = iy$, we have

$$[Q_2^{11}]_{ll'}^{-1} Q_{\text{cs},ll'} \sim e^{(n_1-1)y_1}, \quad (\text{D22})$$

and, for $z = -iy$, we have

$$[Q_2^{11}]_{ll'}^{-1} Q_{cs,ll'} \sim e^{(n_1+1)y_1}. \quad (\text{D23})$$

These equations indicate that $p = 1$ for the outgoing shell wave is satisfactory. For the regular wave given by $[Q_2^{31}]^{-1} Q_{cs}$, we have

$$[Q_2^{31}]_{ll'}^{-1} Q_{cs,ll'} \sim e^{i(1-n_1\alpha)z_1} [a \sin(n_1 z_1) \cos(n_1 z_2) - b \cos(n_1 z_1) \sin(n_1 z_2)]. \quad (\text{D24})$$

For $z = iy$, we have

$$[Q_2^{31}]_{ll'}^{-1} Q_{cs,ll'} \sim e^{-(1-n_1\alpha)y_1} e^{(n_1+n_1\alpha)y_1} = e^{(n_1-1+2n_1\alpha)y_1}, \quad (\text{D25})$$

and, for $z = -iy$, we have

$$[Q_2^{31}]_{ll'}^{-1} Q_{cs,ll'} \sim e^{(1-n_1\alpha)y_1} e^{(n_1+n_1\alpha)y_1} = e^{(n_1+1)y_1}. \quad (\text{D26})$$

Therefore, the regular part can also be expanded with $p = 1$.

APPENDIX E: CAUSALITY AND COMPLETENESS

On the upper half of the complex plane, $\Im(k) > 0$, the response function $R(k)$ of either the homogeneous or core-shell resonator contains no poles due to the causality principle. In the special case of the sphere where $R(k)$ is diagonal, this has been shown to be the valid numerically [15], and we seek to extend this to nonspherical resonators where $R(k)$ is not diagonal. The response matrix on the upper half plane can be written using the Cauchy integral theorem:

$$R(\bar{k}) = \frac{1}{2\pi i} \oint_C dk' \frac{R(k')}{k' - \bar{k}}, \quad (\text{E1})$$

where the contour C is taken to enclose no singularities of the R matrix and \bar{k} is any point lying inside the contour C . We take the contour C to be a semicircle enclosing the whole upper half plane that extends to infinity. It follows that the semicircular path C_R does not contribute to the integration because R vanishes sufficiently fast on the complex plane (i.e., see the asymptotic limits of Q). We are left with only the integration over the real axis

$$R(\bar{k}) = \frac{1}{2\pi i} \int_{-\infty}^{\infty} dk' \frac{R(k')}{k' - \bar{k}}. \quad (\text{E2})$$

Since we want to evaluate R on the real axis, we let $\bar{k} = k + i\delta$ and evaluate the limit as $\delta \rightarrow 0$. For real k , the integral becomes

$$R(k) = \frac{1}{\pi i} P \int_{-\infty}^{\infty} dk' \frac{R(k')}{k' - k}, \quad (\text{E3})$$

where P stands for the principal value integral

$$P \int_{-\infty}^{\infty} dk' \frac{R(k')}{k' - k} = \lim_{\epsilon \rightarrow 0} \left[\int_{-\infty}^{k-\epsilon} dk' \frac{R(k')}{k' - k} + \int_{k+\epsilon}^{\infty} dk' \frac{R(k')}{k' - k} \right]. \quad (\text{E4})$$

Now, we recall the singularity expansion of R in Eq. (D5) went as

$$R(k) = R_0 + \sum_n \frac{R_n}{k - k_n}. \quad (\text{E5})$$

We insert this expansion into Eq. (E3) to obtain

$$R(k) = \frac{R_0}{\pi i} \left(P \int_{-\infty}^{\infty} dk' \frac{1}{k' - k} \right) + \sum_n \frac{R_n}{\pi i} \left(P \int_{-\infty}^{\infty} dk' \frac{1}{(k' - k)(k' - k_n)} \right). \quad (\text{E6})$$

The first integral on the r.h.s. of Eq. (E6) is identically zero,

$$P \int_{-\infty}^{\infty} dk' \frac{1}{k' - k} = 0, \quad (\text{E7})$$

and the second integral on the r.h.s. gives

$$P \int_{-\infty}^{\infty} dk' \frac{1}{(k' - k)(k' - k_n)} = \frac{\pi i}{k - k_n}. \quad (\text{E8})$$

So, on the real-axis, $R(k)$ can be written using only the singularity-dependent part of the expansion

$$R(k) = \sum_n \frac{R_n}{k - k_n}. \quad (\text{E9})$$

This implies the completeness of the QNMs:

$$R(0) + \sum_n \frac{R_n}{k_n} = 0. \quad (\text{E10})$$

APPENDIX F: TOTAL INTERNAL ENERGY

When calculating the internal field energy for lossless materials in the null-field framework, we encounter integrals of the form

$$I_{ll'mm'}^{11} = \frac{1}{V} \int_V dV \mathbf{M}_{lm}(k\mathbf{r}) \cdot \mathbf{M}_{l'm'}^\dagger(k'\mathbf{r}), \quad (\text{F1})$$

where V is the volume of the homogeneous or core-shell resonator. Here the volume integrals of product of SVWFs are transformed into surface integrals enclosing the volume. To proceed in the evaluation Eq. (F1), we recall the identity

$$\nabla \cdot (\mathbf{a} \times \mathbf{b}) = \mathbf{b} \cdot (\nabla \times \mathbf{a}) - \mathbf{a} \cdot (\nabla \times \mathbf{b}), \quad (\text{F2})$$

as well as the divergence theorem

$$\int_V \nabla \cdot \mathbf{F} dV = \oint_S \mathbf{n} \cdot \mathbf{F} dS, \quad (\text{F3})$$

and finally that the SVWFs of polarization type TE and TM are related to each other through

$$\nabla \times \mathbf{M} = k\mathbf{N} \quad \text{and} \quad \nabla \times \mathbf{N} = k\mathbf{M}. \quad (\text{F4})$$

If we now consider the volume integral

$$\begin{aligned} & \int_V \nabla \cdot [\mathbf{M}_{lm}(k\mathbf{r}) \times \mathbf{N}_{l'm'}^\dagger(k'\mathbf{r})] dV \\ &= \int_V [\mathbf{N}_{l'm'}^\dagger(k'\mathbf{r}) \cdot \nabla \times \mathbf{M}_{lm}(k\mathbf{r}) \\ & \quad - \mathbf{M}_{lm}(k\mathbf{r}) \cdot \nabla \times \mathbf{N}_{l'm'}^\dagger(k'\mathbf{r})] dV, \end{aligned}$$

we can use the properties of SVWFs to obtain the following two results:

$$\begin{aligned} & \int_V \nabla \cdot [\mathbf{M}_{lm}(k\mathbf{r}) \times \mathbf{N}_{l'm'}(k'\mathbf{r})] dV \\ &= \int_V k \mathbf{N}_{l'm'}(k'\mathbf{r}) \cdot \mathbf{N}_{lm}(k\mathbf{r}) - k' \mathbf{M}_{lm}(k\mathbf{r}) \cdot \mathbf{M}_{l'm'}(k'\mathbf{r}) dV, \end{aligned} \quad (\text{F5})$$

$$\begin{aligned} & \int_V \nabla \cdot [\mathbf{N}_{lm}(k\mathbf{r}) \times \mathbf{M}_{l'm'}(k'\mathbf{r})] dV \\ &= \int_V k \mathbf{M}_{l'm'}(k'\mathbf{r}) \cdot \mathbf{M}_{lm}(k\mathbf{r}) - k' \mathbf{N}_{lm}(k\mathbf{r}) \cdot \mathbf{N}_{l'm'}(k'\mathbf{r}) dV. \end{aligned} \quad (\text{F6})$$

The volume integrals $\int_V \mathbf{N}_{lm}(k\mathbf{r}) \cdot \mathbf{N}_{l'm'}(k'\mathbf{r}) dV$ can be eliminated by adding the product of k' and Eq. (F5) to the product of k and Eq. (F6). That result can be reorganized as

$$\begin{aligned} & (k^2 - k'^2) \int_V \mathbf{M}_{lm}(k\mathbf{r}) \cdot \mathbf{M}_{l'm'}^\dagger(k'\mathbf{r}) dV \\ &= k \int_V \nabla \cdot [\mathbf{N}_{lm}(k\mathbf{r}) \times \mathbf{M}_{l'm'}^\dagger(k'\mathbf{r})] dV \\ &+ k' \int_V \nabla \cdot [\mathbf{M}_{lm}(k\mathbf{r}) \times \mathbf{N}_{l'm'}^\dagger(k'\mathbf{r})] dV, \end{aligned}$$

where we note the dagger is the Hermitian conjugate, which, for lossless materials and real frequencies, only conjugates the angular part of the SVWF. Dividing both sides by $V(k^2 - k'^2)$ and taking the limit, we get

$$\begin{aligned} & I_{ll'mm'}^{11}(k) \\ &= \frac{1}{V} \lim_{k' \rightarrow k} \frac{k}{k^2 - k'^2} \int_V \nabla \cdot [\mathbf{N}_{lm}(k\mathbf{r}) \times \mathbf{M}_{l'm'}^\dagger(k'\mathbf{r})] dV \\ &+ \frac{1}{V} \lim_{k' \rightarrow k} \frac{k'}{k^2 - k'^2} \int_V \nabla \cdot [\mathbf{M}_{lm}(k\mathbf{r}) \times \mathbf{N}_{l'm'}^\dagger(k'\mathbf{r})] dV. \end{aligned}$$

Applying the divergence theorem, the volume integrals can be transformed into surface integrals:

$$\begin{aligned} & I_{ll'mm'}^{11}(k) \\ &= \frac{1}{V} \lim_{k' \rightarrow k} \frac{k}{k^2 - k'^2} \oint_S \mathbf{n} \cdot [\mathbf{N}_{lm}(k\mathbf{r}) \times \mathbf{M}_{l'm'}^\dagger(k'\mathbf{r})] dS \\ &+ \frac{1}{V} \lim_{k' \rightarrow k} \frac{k'}{k^2 - k'^2} \oint_S \mathbf{n} \cdot [\mathbf{M}_{lm}(k\mathbf{r}) \times \mathbf{N}_{l'm'}^\dagger(k'\mathbf{r})] dS. \end{aligned} \quad (\text{F7})$$

Similar results can be found for the integrals that involve SVWFs of a different polarization type. It turns out the

limit at $k' = k$ can be evaluated explicitly by expanding out the terms in the integrand accordingly. When the need arises, L'Hôpital's rule was invoked to calculate the limit. The Hermitian matrix $I(k)$ comprises four block matrices that encompass the polarization interactions

$$I = \begin{bmatrix} I^{11} & I^{12} \\ I^{21} & I^{22} \end{bmatrix}, \quad (\text{F8})$$

where the first block matrix was given above. The fourth block matrix is

$$\begin{aligned} & I_{ll'mm'}^{22}(k) \\ &= \frac{1}{V} \lim_{k' \rightarrow k} \frac{k'}{k^2 - k'^2} \oint_S \mathbf{n} \cdot [\mathbf{N}_{lm}(k\mathbf{r}) \times \mathbf{M}_{l'm'}^\dagger(k'\mathbf{r})] dS \\ &+ \frac{1}{V} \lim_{k' \rightarrow k} \frac{k}{k^2 - k'^2} \oint_S \mathbf{n} \cdot [\mathbf{M}_{lm}(k\mathbf{r}) \times \mathbf{N}_{l'm'}^\dagger(k'\mathbf{r})] dS, \end{aligned} \quad (\text{F9})$$

and with $I^{12} = [I^{21}]^\dagger$, the second block matrix is

$$\begin{aligned} & I_{ll'mm'}^{12}(k) \\ &= \frac{1}{V} \lim_{k' \rightarrow k} \frac{k'}{k^2 - k'^2} \oint_S \mathbf{n} \cdot [\mathbf{M}_{lm}(k\mathbf{r}) \times \mathbf{M}_{l'm'}^\dagger(k'\mathbf{r})] dS \\ &+ \frac{1}{V} \lim_{k' \rightarrow k} \frac{k}{k^2 - k'^2} \oint_S \mathbf{n} \cdot [\mathbf{N}_{lm}(k\mathbf{r}) \times \mathbf{N}_{l'm'}^\dagger(k'\mathbf{r})] dS. \end{aligned} \quad (\text{F10})$$

To calculate the total internal energy of a core-shell resonator, the volume integral is separated into the core and shell contributions, with the shell contribution comprised a surface integral evaluated on the core-shell interface, and the other on the resonator surface. In the case of a homogeneous spherical resonator with a size parameter x , we recover the following known expressions [15,21]:

$$\begin{aligned} I_l^{11} &= \frac{3}{8\pi(nx)^3} \left\{ nx[\psi_l'(nx)]^2 \right. \\ &\quad \left. - \psi_l'(nx)\psi_l(nx) + nx \left[1 - \frac{l(l+1)}{(nx)^2} \right] [\psi_l(nx)]^2 \right\}, \end{aligned} \quad (\text{F11})$$

$$\begin{aligned} I_l^{22} &= \frac{3}{8\pi(nx)^3} \left\{ nx[\psi_l'(nx)]^2 \right. \\ &\quad \left. + \psi_l'(nx)\psi_l(nx) + nx \left[1 - \frac{l(l+1)}{(nx)^2} \right] [\psi_l(nx)]^2 \right\}. \end{aligned} \quad (\text{F12})$$

[1] P. Lalanne, W. Yan, K. Vynck, C. Sauvan, and J.-P. Hugonin, Light interaction with photonic and plasmonic resonances, *Laser Photonics Rev.* **12**, 1700113 (2018).
 [2] Y. B. Zel'Dovich, On the theory of unstable states, *Sov. Phys. JETP* **12**, 542 (1961).
 [3] H. M. Lai, P. T. Leung, K. Young, P. W. Barber, and S. C. Hill, Time-independent perturbation for leaking electromagnetic modes in open systems with application to resonances in microdroplets, *Phys. Rev. A* **41**, 5187 (1990).

[4] W. Yan, R. Faggiani, and P. Lalanne, Rigorous modal analysis of plasmonic nanoresonators, *Phys. Rev. B* **97**, 205422 (2018).
 [5] M. B. Doost, W. Langbein, and E. A. Muljarov, Resonant-state expansion applied to three-dimensional open optical systems, *Phys. Rev. A* **90**, 013834 (2014).
 [6] Q. Bai, M. Perrin, C. Sauvan, J.-P. Hugonin, and P. Lalanne, Efficient and intuitive method for the analysis of light scattering by a resonant nanostructure, *Opt. Express* **21**, 27371 (2013).

- [7] F. Alpeggiani, N. Parappurath, E. Verhagen, and L. Kuipers, Quasinormal-Mode Expansion of the Scattering Matrix, *Phys. Rev. X* **7**, 021035 (2017).
- [8] S. Franke, S. Hughes, M. K. Dezfouli, P. T. Kristensen, K. Busch, A. Knorr, and M. Richter, Quantization of Quasinormal Modes for Open Cavities and Plasmonic Cavity Quantum Electrodynamics, *Phys. Rev. Lett.* **122**, 213901 (2019).
- [9] A. Doicu, T. Wriedt, and Y. A. Eremin, *Light Scattering by Systems of Particles: Null-Field Method with Discrete Sources: Theory and Programs*, Optical Sciences, Vol. 124 (Springer, Berlin, 2006).
- [10] P. Barber and C. Yeh, Scattering of electromagnetic waves by arbitrarily shaped dielectric bodies, *Appl. Opt.* **14**, 2864 (1975).
- [11] P. C. Waterman, Matrix formulation of electromagnetic scattering, *Proc. IEEE* **53**, 805 (1965).
- [12] C. Baum, Emerging technology for transient and broad-band analysis and synthesis of antennas and scatterers, *Proc. IEEE* **64**, 1598 (1976).
- [13] D. A. Powell, Interference Between the Modes of an All-Dielectric Meta-Atom, *Phys. Rev. Applied* **7**, 034006 (2017).
- [14] V. Grigoriev, A. Tahri, S. Varault, B. Rolly, B. Stout, J. Wenger, and N. Bonod, Optimization of resonant effects in nanostructures via Weierstrass factorization, *Phys. Rev. A* **88**, 011803(R) (2013).
- [15] R. Colom, R. McPhedran, B. Stout, and N. Bonod, Modal expansion of the scattered field: Causality, nondivergence, and nonresonant contribution, *Phys. Rev. B* **98**, 085418 (2018).
- [16] B. Stout, R. Colom, N. Bonod, and R. C. McPhedran, Spectral expansions of open and dispersive optical systems: Gaussian regularization and convergence, *New J. Phys.* **23**, 083004 (2021).
- [17] A. E. Miroshnichenko, A. B. Evlyukhin, Y. F. Yu, R. M. Bakker, A. Chipouline, A. I. Kuznetsov, B. Luk'yanchuk, B. N. Chichkov, and Y. S. Kivshar, Nonradiating anapole modes in dielectric nanoparticles, *Nat. Commun.* **6**, 8069 (2015).
- [18] B. Luk'yanchuk, R. Paniagua-Domínguez, A. I. Kuznetsov, A. E. Miroshnichenko, and Y. S. Kivshar, Hybrid anapole modes of high-index dielectric nanoparticles, *Phys. Rev. A* **95**, 063820 (2017).
- [19] A. K. Ospanova, A. Basharin, A. E. Miroshnichenko, and B. Luk'yanchuk, Generalized hybrid anapole modes in all-dielectric ellipsoid particles, *Opt. Mater. Express* **11**, 23 (2021).
- [20] A. Canós Valero, E. A. Gurvitz, F. A. Benimetskiy, D. A. Pidgayko, A. Samusev, A. B. Evlyukhin, V. Bobrovs, D. Redka, M. I. Tribelsky, M. Rahmani, K. Z. Kamali, A. A. Pavlov, A. E. Miroshnichenko, and A. S. Shalin, Theory, observation, and ultrafast response of the hybrid anapole regime in light scattering, *Laser Photonics Rev.* **15**, 2100114 (2021).
- [21] R. Colom, R. McPhedran, B. Stout, and N. Bonod, Modal analysis of anapoles, internal fields, and Fano resonances in dielectric particles, *J. Opt. Soc. Am. B* **36**, 2052 (2019).
- [22] A. Doicu and M. I. Mishchenko, An overview of the null-field method. I: Formulation and basic results, *Phys. Open* **5**, 100020 (2020).
- [23] W. Heiss, The physics of exceptional points, *J. Phys. A: Math. Theor.* **45**, 444016 (2012).
- [24] C. Sauvan, Quasinormal modes expansions for nanoresonators made of absorbing dielectric materials: Study of the role of static modes, *Opt. Express* **29**, 8268 (2021).
- [25] R. Friehmelt and S. Heidenreich, Calibration of a white-light/90° optical particle counter for “aerodynamic” size measurements experiments and calculations for spherical particles and quartz dust, *J. Aerosol Sci.* **30**, 1271 (1999).
- [26] H. M. Lai, C. C. Lam, P. T. Leung, and K. Young, Effect of perturbations on the widths of narrow morphology-dependent resonances in mie scattering, *J. Opt. Soc. Am. B* **8**, 1962 (1991).
- [27] E. Bulgakov, K. Pichugin, and A. Sadreev, Exceptional points in a dielectric spheroid, *Phys. Rev. A* **104**, 053507 (2021).
- [28] D. Riley, A simple and accurate resonance expansion for the electromagnetic field scattered by a lossy dielectric sphere, *IEEE Trans. Antennas Propag.* **34**, 737 (1986).
- [29] W. Somerville, B. Auguié, and E. Le Ru, Smarties: User-friendly codes for fast and accurate calculations of light scattering by spheroids, *J. Quant. Spectrosc. Radiat. Transfer* **174**, 39 (2016).
- [30] C. F. Bohren and D. R. Huffman, *Absorption and Scattering of Light by Small Particles* (Wiley-VCH, 1983), p. 28.
- [31] M. E. Rose, *Multipole Fields* (Wiley, New York, 1955), p. 25.
- [32] L. Hogben, *Handbook of Linear Algebra* (CRC Press, 2006).
- [33] L. Delves and J. Lyness, A numerical method for locating the zeros of an analytic function, *Math. Comp.* **21**, 543 (1967).
- [34] T. C. Preston and J. P. Reid, Determining the size and refractive index of microspheres using the mode assignments from Mie resonances, *J. Opt. Soc. Am. A* **32**, 2210 (2015).
- [35] B. Vennes and T. C. Preston, Calculating and fitting morphology-dependent resonances of a spherical particle with a concentric spherical shell, *J. Opt. Soc. Am. A* **36**, 2089 (2019).